

Optimal custom design of both symmetric and unsymmetrical hexapod robots for aeronautics applications

Andrea Cirillo ^a, Pasquale Cirillo ^{a,*}, Giuseppe De Maria ^a, Alessandro Marino ^b, Ciro Natale ^a, Salvatore Pirozzi ^a

^a Seconda Università degli Studi di Napoli, Dipartimento di Ingegneria Industriale e dell'Informazione, Via Roma, 29, 81031 Aversa, Italy

^b Università degli Studi di Salerno, Dipartimento di Ingegneria dell'Informazione ed Elettrica e Matematica Applicata, Via Giovanni Paolo II, 132, 84084 Fisciano, Italy

ARTICLE INFO

Article history:

Received 8 June 2015

Received in revised form

2 June 2016

Accepted 24 June 2016

Keywords:

Aeronautics part positioning

Adaptive fixture

Stewart platform

Parallel robot

Optimal design

Genetic algorithm

ABSTRACT

The Stewart parallel mechanism is used in various applications due to its high load-carrying capacity, accuracy and stiffness, such as flight simulation, spaceship aligning, radar and satellite antenna orientation, rehabilitation applications, parallel machine tools. However, the use of such parallel robots is not widespread due to three factors: the limited workspace, the singularity configurations existing inside the workspace, and the high cost. In this work, an approach to support the design of a cost-effective Stewart platform-based mechanism for specific applications and to facilitate the choice of suitable components (e.g., linear actuators and base and mobile plates) is presented. The optimal design proposed in this work has multiple objectives. In detail, it intends to maximize the payload and minimize the forces at each leg needed to counteract external forces applied to the mobile platform during positioning or manufacturing, or, in general, during specific applications. The approach also aims at avoiding reduction of the robot workspace through a kinematic optimization. Both symmetric and unsymmetrical geometries have been analysed to show how the optimal design approach can lead to effective results with different robot configurations. Moreover, these objectives are achieved through a dynamic optimization and several optimization algorithms were compared in terms of defined performance indexes.

© 2016 Elsevier Ltd. All rights reserved.

1. Introduction

Nowadays, the assembly process of aircrafts highly relies on skilled human operators that are necessary in all the assembly phases, such as part positioning, drilling, fastening, riveting, and quality assurance. With the introduction of the composite and reinforced carbon fiber technologies into the manufacturing process, the aeronautics industry is experiencing an increase of the non-added value operations (i.e., temporary assembly to check gaps, shimming, dismantling, tool handling, drilling, and fastening) that lead to an increase of the overall manufacturing costs and, principally, of the overall process time. In this field, the research is focusing on the development of cost efficient part manufacturing and assembly processes of composite, metal and hybrid airframe structures. Their introduction in the manufacturing process aims to the reduction or the total elimination of the most time consuming and hence expensive operations. In order to achieve a lean manufacturing process and ensure the accuracy and the

repeatability required in the aeronautics standards, new co-shared manual and automated operations are under investigation. Several riveting and drilling solutions that make use of complex and heavy multi-function end effector and oversized industrial robots have been proposed in the literature [1–8], but only few solutions have been proposed for the aeronautics part positioning problem [9–11]. The conventional assembly process requires that the parts to manufacture are positioned into welded mechanical structures, called fixtures. A fixture is a work-holding or support device used to securely locate (in a specific location or orientation) and support the work, ensuring that all parts produced using the fixture will maintain conformity and interchangeability. Therefore, the fixtures are designed on the base of the considered aircraft subsection, e.g., wing-box, fuselage; changes in the held parts could result in changes in the fixture that could cause an increase of the manufacturing process costs and introduce a delay in the overall manufacturing line. The ability to change the configuration of an airframe assembly tool in order to assemble different products within a product family becomes a very important feature. Reconfigurable tooling should reduce the number of tools on the workshop floor and, thereby, save floor space; it should simplify the build-up and change of assembly tools and drastically reduce

* Corresponding author.

E-mail address: pasquale.cirillo@unina2.it (P. Cirillo).



lead time in tooling design and build-up. The solutions proposed in the literature use standardized profiles, which make the fixtures possible to re-cycle the parts, and as the parts in the fixture are not welded, they can be adjusted and provide some flexibility. There also exist techniques to achieve reconfigurability by using the so-called pogo sticks, which can change the configuration to adapt themselves according to the specific airframe structures [12]. In recent years, the research is focusing on the development of adaptive fixtures which make use of parallel robots, i.e., Stewart platform-based robots, to position or to hold the parts during the manufacturing/assembling phases [13]. In comparison with a serial manipulator, the Stewart parallel manipulator, capable of providing six degrees of freedom (DOF) movement, comes up with some advantages [14] that make them the optimal solution for these types of applications:

- high strength and stiffness-to-weight ratios can be achieved since the links do not carry moment loads but act only in tension and compression;
- positioning of the end effector is performed by actuators acting in parallel, resulting in a total force and moment capability greater than each individual servomechanism;
- moving only the end effector in space rather than massive servomechanisms results in economy of power, excellent dynamic performance, and low manipulator inertia;
- high accuracy and precision is possible since actuator errors are not magnified by lengthy linkages.

In fact, the Stewart platform, also called hexapod, is used in many applications where high positioning accuracy and high stiffness are required, i.e., flight simulation [15], spaceship aligning, radar and satellite antenna orientation [16,17], rehabilitation applications [18], robots [19], and parallel machine tools [20,21]. Unfortunately, there are factors that limit and complicate the design of such a mechanism. First, the limited workspace that reduces the number of tasks the robot can execute and the singularity configurations existing inside the workspace in which the manipulator gains one or more degrees of freedom and therefore loses its stiffness. The closed-loop nature of parallel mechanisms generates complex singularities inside the workspace, which makes the workspace analysis and the trajectory planning of parallel mechanisms a challenge. Moreover, although the versatility of the hexapod has been recognized, its acceptance by industry as production equipment has not yet occurred. Some obstacles to this include the high cost and unproven performance in a production environment for a specific task. Hence, the design of an efficient approach that allows us to maximize the robot workspace, reduces the singularities inside the workspace, optimizes the design of the parallel platform reducing the hexapod costs, and keeps limited its encumbrance becomes a very important issue.

2. Problem formulation

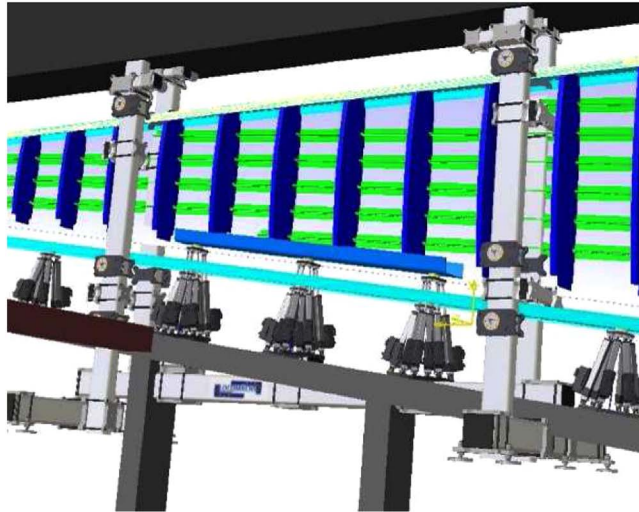
In order to better understand the versatility of the use of the Stewart platforms in the aeronautics assembly/manufacturing process, a brief review on the general aeronautics build philosophy is reported. The conventional vertical manual approach used in the aircraft assembly is a time-consuming and labor-intensive process that requires several and subsequent phases of assembling and disassembling in order to accurately position the aeronautics parts. Once all the parts are positioned inside the fixture, an intensive shimming phase is carried out in order to increase the coupling before the clamping and the drilling phases and, thus, to ensure that the final product respects the tolerances specified in the mechanical drawings. After the shimming phase, a clamping

phase is carried out by using a large number of temporary fasteners to assure the perfect coupling between the parts before the drilling phase. Finally, the drilling and the riveting tasks can be performed. The aeronautics researchers have proposed new technologies to reduce the shimming time, e.g., by automatically creating the shims before mounting the parts on the fixture. Moreover, as already illustrated in Section 1, valid automated solutions for aeronautics riveting and drilling have been proposed [22]. The positioning problem, instead, is an open research field and only few applications using hexapods inside the aeronautics fixture can be found [13]. An adaptive and flexible fixture constituted by Stewart platforms can be exploited, for example, in the positioning and holding of the airframe parts during a manufacturing process, e.g., riveting and drilling. The spar and rib positioning are two of the many applications in which the use of the hexapod can be exploited. In both the aforementioned problems, it is required that the airframe part is accurately positioned into the fixture, with a perfect coupling between the other parts, i.e., upper and lower covers, ribs and stringers. Furthermore, in the positioning phase, it must be guaranteed that the moved part does not collide with the other parts in the fixture to prevent damages and possible material deformations. When the part is in its final position, often, a drilling process is carried out through more coupled parts in order to reduce the coupling problems that may occur in the next assembly phases.

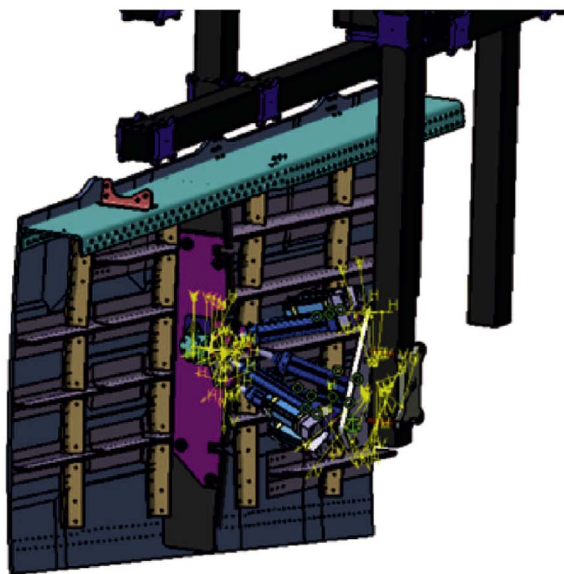
In this scenario, a lot of machining tools are involved, so, it is important to reduce the encumbrance of the parallel machines used to keep and move the parts during the entire assembly process in order to avoid the insertion and removal of the tool inside the airframe fixture and collisions between the machining tools. At the same time, it is important to take into account the external forces acting on the platforms during the process, and the dimensions and the weight of the part to position for better dimensioning the platforms and to satisfy the strict aeronautics manufacturing requirements. High forces applied on the robot top plate, e.g., during the drilling phase or the riveting phase, can deflect the robot end effector and, then, reduce the positioning accuracy in such a way that the resulting holes are outside of specified tolerances. Moreover, in order to reduce the fastening time and, at the same time, ensure high manufacturing quality, the parallel robot can be exploited to apply a clamping force to airframe parts opposing to the drilling or riveting actions through the use of a force sensor and a force control.

Fig. 1 shows a concept of a flexible/adaptative fixture designed to overcome the aforementioned issues (the 3D drawings are parts of the demonstrator of the LOCOMACHS project). In particular, the picture on the top shows a possible use of three cooperative Stewart platforms for the spar positioning; on the bottom image, a Stewart platform is used into a flexible fixture for positioning a rib into the wingbox during the assembly process.

The presented work provides an approach to support the design of n hexapod machines to be used in such applications that impose strict criteria in terms of high positioning accuracy and, at the same time, dimension constraints and low cost. In this context, it is important to take into account also the forces acting on the platform during the whole task. Therefore, the main issue is the reduction of the size of the platform and, simultaneously, increase the maximum external force that can be counteracted by the platform during a machining task. This is not a trivial issue, since the reduction of the platform dimensions implies also the reduction of the actuator dimensions, and, thus, of their maximum load. Moreover, by reducing the plate dimensions, the leg configuration changes, and this could lead to a reduction of the stiffness and the accuracy of the parallel robot. According to the previous discussion, an alternative



(a) Spar positioning.



(b) Rib positioning.

Fig. 1. Part positioning tasks.

approach to support the design of a low cost Stewart platform-based mechanism for manufacturing applications is proposed in this work. The approach allows the user to optimize the design of the Stewart platform based on the performance and criteria required by the desired application, by adjusting the leg attachment points on both top and base plates making use of both a dynamic and kinematic optimization. A dynamic optimization is carried out to maximize the payload and improve the rejection of external forces exerted on the mobile platform during positioning or manufacturing applications, while, in order to avoid reduction of the robot workspace, also a kinematic optimality criterion is considered in the optimization process as well. Moreover, the leg attachment points on either mobile (or top) and fixed (or base) plates are optimized satisfying the mechanical constraints introduced in the design (such as leg attachment point geometry, distances between the legs/actuators, minimum and maximum top and base plate dimensions, minimum and maximum leg strokes).

In detail, an optimization algorithm is used to combine two or more different optimum objectives by properly defining a cost function to minimize. In order to minimize the maximum leg force value and to equally distribute among the legs the forces exerted by the linear actuators during a positioning and/or machining task, the maximum root-mean-square (RMS) value of the forces is selected as optimum objective. A second optimum objective has been taken into account to maximize (or do not penalize) the robot workspace volume. In order to select the most suitable optimization algorithm for the proposed application, different algorithms have been compared. The performances of the Genetic Algorithm (GA) [23,24], the Sequential Quadratic Programming (SQP) algorithm [25–28], the Multi-Start algorithm and the Global Search algorithm [29–31] have been analysed and compared. As it will be detailed in the following, the comparison shows that the GA provides better results than the other ones in terms of minimum found cost function values and number of cost function evaluations. Finally, in order to exploit the anisotropic property of the parallel robot and better optimize the mechanical design given a specific task, the Stewart platform optimization process has been carried out by considering both symmetric and unsymmetrical geometries. All the proposed results have been obtained by considering specific tasks for a single hexapod: positioning and drilling tasks are simulated in order to consider two of the most common manufacturing processes in aeronautics.

3. Related work

During the past decade, the structural design and optimization of Stewart platform represented two topics of great interest for researchers. Given the number of performance parameters to consider (i.e., workspace volume, manipulability, dexterity, singularity, accuracy, actuators interference, actuation forces) it is still difficult to find an optimal general design for a 6-DOF parallel manipulator. Design optimization and dimensional synthesis of the parallel mechanism has been presented as a multi-criteria constrained problem in [32–38]. In the optimization process, kinematic parameters are usually considered, i.e., workspace [38–47], stiffness [48–51], dexterity [38,52,53], singularity [17,54,42,43], maximum end-effector velocity [55], and manipulability [56]. In the literature, several approaches to the dynamic optimal design of parallel robots take into consideration criteria such as balance [19,57–60] and torque indexes [19,61], but there are few works that deal with the issues of the anisotropic property [62,55] of parallel robot or that consider criteria such as acceleration, velocity, gravity and external force components in the considered cost function. Those issues are well explained in [61]. In the existing literature, the isotropy property is usually pursued in the dimensional synthesis of the parallel robot. But it is known that most of the parallel robots with symmetrical structures have not isotropic performance in the whole workspace since they have not the same capability in all directions [60,63]. It is important to emphasize the fact that also the performance requirements of the parallel robot are usually not uniform in all directions within the entire desired workspace in practical and specific applications. Thus, the anisotropic property should be considered in the dimensional synthesis of the parallel robot with the aim to obtain a more suitable optimal design. Furthermore, the objective function of the dynamic optimal design of the parallel robot is usually based on the generalized inertia matrix, which describes the mapping between the joint forces/torques and the accelerations. The velocity, gravity and the external force components are not considered in the above objective functions. On the other hand,

the velocity components should be taken into account when the parallel robot is used for high speed operations, the gravity forces should be considered when the parallel robot is involved in heavy load situation, the external force component should be considered when the parallel robot is used for machining operation.

This work is aimed at optimizing the Stewart platform design by modeling the entire system by means of a physics-based approach. In the inverse dynamics computation, the gravity contribution, the external forces acting on the platform during the execution of the performed task, as well as the inertia matrix, have been considered, while, kinematic parameters such as the workspace and dynamics criteria such as balance have been combined in the cost function described in [Section 5.1](#). The optimization process has been carried out along a specific trajectory, generated to simulate typical aeronautics assembly phases, e.g., positioning and drilling/riveting processes (illustrated in [Section 2](#)), comparing the results obtained by considering isotropic and anisotropic platform geometries. Finally, constraining the search domain, also the encumbrance of the platform can be reduced.

4. The hexapod geometry

The proposed approach adopts a simulation environment to support the design of a Stewart platform-based mechanism for specific applications. A dynamic optimization is carried out to minimize a cost function that will be defined in [Section 5.1](#). Different from many existing approaches, the optimization makes use of the dynamics of the hexapod and computes the inverse dynamics (ID) in order to check at each iteration the forces required to the legs. Given an initial configuration of the Stewart platform in terms of leg attachment points on base and top plates and given two sets of bounds properly defined on the base of the mechanical constraints, a GA is used to solve a nonlinear constrained problem. The bounds are defined for each leg attachment point and delimit the area in which the points can be moved during the optimization process. They should be defined to avoid collisions between the legs, actuators and fixtures, to satisfy specified maximum dimensions of the plates or other mechanical constraints. In other words, the Stewart platform is optimized by adjusting the leg attachment points $\mathbf{a}_i = [a_{x_i}, a_{y_i}]^T$ and $\mathbf{b}_i = [b_{x_i}, b_{y_i}]^T$ on the base and top plate minimizing the selected cost function, respectively (see [Fig. 2](#)). The vectors \mathbf{a}_i and \mathbf{b}_i represent the vector of the Cartesian coordinates of the leg attachment points expressed in base frame and top frame, respectively, and they can be parameterized on the base of the considered geometry as illustrated in [Section 4.1](#).

4.1. Parameterizations of the hexapod geometries

In this section, the parametrization defined to represent the hexapod geometries used in the optimization process illustrated in [Section 5](#) is presented. In order to find the best geometry providing, at the same time,

- the maximum workspace volume,
- the minimum value of the leg forces exerted by the actuators,
- the minimum dimensions of the platform,

several symmetric and unsymmetrical hexapod geometries have been evaluated for the optimization process. The choice of

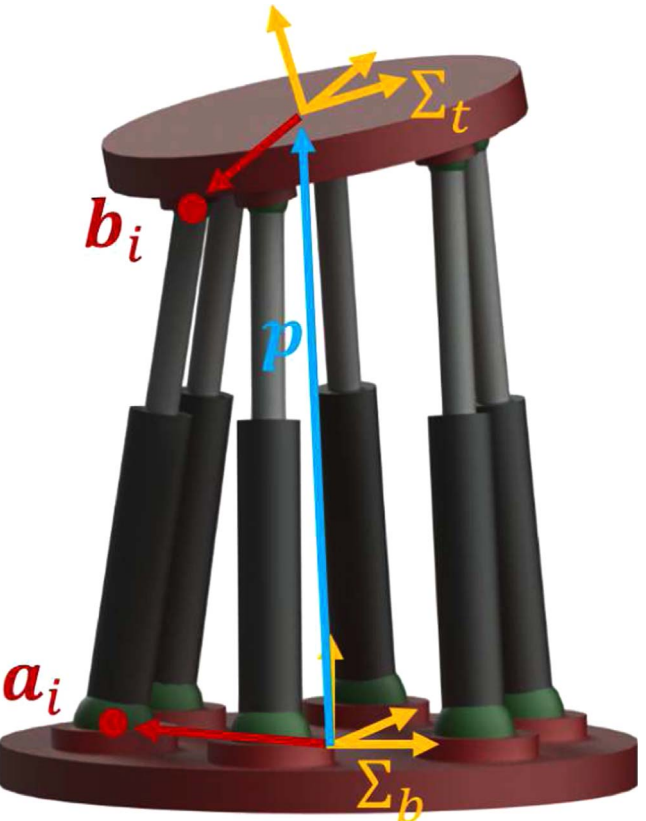


Fig. 2. General Stewart platform scheme.

the geometry also affects the time required for the optimization process: the use of a large number of variables allows us to optimize the platform minimizing the number of constraints but it increases the computational time. The Stewart–Gough, Griffis–Duffy [64] and MSP [32] geometries and the more general one-axis geometry [19] were investigated. Note that a drawback of the original Stewart platform design is that, due to interference constraints between the legs, the orientations of the legs cannot deviate far from the z -axis of the manipulator. Since the static force applied by each leg to the moving platform must act along the axis of the leg, the force capacity in the z direction is considerably higher than the force capacity in the x – y plane, and the torque capacity about the z -axis is limited. Such issue is partially solved in the Griffis–Duffy geometry and in the MSP geometry, hence, they are considered in the proposed analysis.

The aforementioned geometries are briefly recalled in the following.

4.1.1. Stewart–Gough geometry (4 variables) – symmetric geometry (SG4)

The geometry is defined by using two variables for the base plate and two variables for the top plate (see [Fig. 3](#)). In particular, ρ_b and ρ are the circle radius of the base and top plates, respectively, and θ_{hb} and θ_h are the half angle between two pairs of joints on the base and on the top plates, respectively. So, the vector of the unknown variables can be written as $\mathbf{x} = [\theta_{hb} \ \theta_h \ \rho_b \ \rho]^T$. The leg attachment point positions \mathbf{a}_i and \mathbf{b}_i , with respect to base frame and mobile frame, can be easily computed in the Cartesian space as a function of the geometry parameters defined above as reported below:

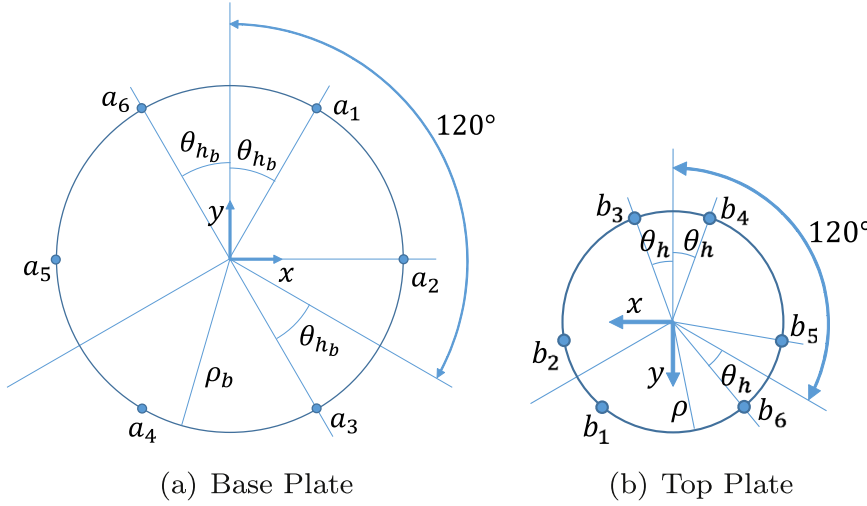


Fig. 3. Stewart-Gough platform 4 variables geometry.

$$\begin{aligned}
 a_{x_1} &= \rho_b \cos\left(\frac{\pi}{2} - \theta_{hb}\right), & a_{y_1} &= \rho_b \sin\left(\frac{\pi}{2} - \theta_{hb}\right) \\
 a_{x_2} &= \rho_b \cos\left(-\frac{\pi}{6} + \theta_{hb}\right), & a_{y_2} &= \rho_b \sin\left(-\frac{\pi}{2} + \theta_{hb}\right) \\
 a_{x_3} &= \rho_b \cos\left(-\frac{\pi}{6} - \theta_{hb}\right), & a_{y_3} &= \rho_b \sin\left(-\frac{\pi}{6} - \theta_{hb}\right) \\
 a_{x_4} &= \rho_b \cos\left(-\frac{5}{6}\pi + \theta_{hb}\right), & a_{y_4} &= \rho_b \sin\left(-\frac{5}{6}\pi + \theta_{hb}\right) \\
 a_{x_5} &= \rho_b \cos\left(-\frac{5}{6}\pi - \theta_{hb}\right), & a_{y_5} &= \rho_b \sin\left(-\frac{5}{6}\pi - \theta_{hb}\right) \\
 a_{x_6} &= \rho_b \cos\left(\frac{\pi}{2} + \theta_{hb}\right), & a_{y_6} &= \rho_b \sin\left(\frac{\pi}{2} + \theta_{hb}\right) \\
 b_{x_1} &= \rho \cos\left(\frac{\pi}{2} - \theta_h\right), & b_{y_1} &= \rho \sin\left(\frac{\pi}{2} - \theta_h\right) \\
 b_{x_2} &= \rho \cos\left(-\frac{\pi}{6} + \theta_h\right), & b_{y_2} &= \rho \sin\left(-\frac{\pi}{2} + \theta_h\right) \\
 b_{x_3} &= \rho \cos\left(-\frac{\pi}{6} - \theta_h\right), & b_{y_3} &= \rho \sin\left(-\frac{\pi}{6} - \theta_h\right) \\
 b_{x_4} &= \rho \cos\left(-\frac{5}{6}\pi + \theta_h\right), & b_{y_4} &= \rho \sin\left(-\frac{5}{6}\pi + \theta_h\right) \\
 b_{x_5} &= \rho \cos\left(-\frac{5}{6}\pi - \theta_h\right), & b_{y_5} &= \rho \sin\left(-\frac{5}{6}\pi - \theta_h\right) \\
 b_{x_6} &= \rho \cos\left(\frac{\pi}{2} + \theta_h\right), & b_{y_6} &= \rho \sin\left(\frac{\pi}{2} + \theta_h\right).
 \end{aligned} \tag{1}$$

Note that only x and y coordinates are considered since the z coordinate is fixed by the mechanical design.

4.1.2. Stewart-Gough geometry (8 variables) – unsymmetric geometry (SG8)

The previous geometry can be modified as in Fig. 4 by relaxing some constraints and by defining each leg attachment point position individually. Four variables are used to define the leg attachment points on the base plate and other four variables are used to define the leg attachment points on the top plate. In particular, ρ_b and ρ are the circle radii of the base and top plates, respectively; θ_{ai} and θ_{bi} with $i = 1, 2, 3$ are the angles that define the three joint positions in the half-plane of the positive x -axis on the base plate and on the top plate, respectively. The joint positions of the three legs in the left half-plane are calculated by symmetry with respect to the y -axis. The vector containing the unknown variables is $\mathbf{x} = [\theta_{a1} \ \theta_{a2} \ \theta_{a3} \ \theta_{b1} \ \theta_{b2} \ \theta_{b3} \ \rho_b \ \rho]^T$. The leg

attachment point positions, with respect to the base plate frame and top plate frame, can be computed in the Cartesian space as a function of the parameters just defined:

$$\begin{aligned}
 a_{x_1} &= \rho_b \cos(\theta_{a1}), & a_{y_1} &= \rho_b \sin(\theta_{a1}) \\
 a_{x_2} &= \rho_b \cos(\theta_{a2}), & a_{y_2} &= \rho_b \sin(\theta_{a2}) \\
 a_{x_3} &= \rho_b \cos(\theta_{a3}), & a_{y_3} &= \rho_b \sin(\theta_{a3}) \\
 a_{x_4} &= \rho_b \cos(\pi - \theta_{a3}), & a_{y_4} &= \rho_b \sin(\pi - \theta_{a3}) \\
 a_{x_5} &= \rho_b \cos(\pi - \theta_{a2}), & a_{y_5} &= \rho_b \sin(\pi - \theta_{a2}) \\
 a_{x_6} &= \rho_b \cos(\pi - \theta_{a1}), & a_{y_6} &= \rho_b \sin(\pi - \theta_{a1}) \\
 b_{x_1} &= \rho \cos(\theta_{b1}), & b_{y_1} &= \rho \sin(\theta_{b1}) \\
 b_{x_2} &= \rho \cos(\theta_{b2}), & b_{y_2} &= \rho \sin(\theta_{b2}) \\
 b_{x_3} &= \rho \cos(\theta_{b3}), & b_{y_3} &= \rho \sin(\theta_{b3}) \\
 b_{x_4} &= \rho \cos(\pi - \theta_{b3}), & b_{y_4} &= \rho \sin(\pi - \theta_{b3}) \\
 b_{x_5} &= \rho \cos(\pi - \theta_{b2}), & b_{y_5} &= \rho \sin(\pi - \theta_{b2}) \\
 b_{x_6} &= \rho \cos(\pi - \theta_{b1}), & b_{y_6} &= \rho \sin(\pi - \theta_{b1}).
 \end{aligned} \tag{2}$$

4.1.3. Generic one-axis geometry (12 variables) – unsymmetrical geometry (OA12)

The leg attachment points are defined in the Cartesian space (see Fig. 5). The geometry parameters are the x and y coordinates a_{xi} , a_{yi} , b_{xi} , b_{yi} with $i = 1, 2, 3$ of the leg positions in the half-plane of the positive x -axis on the base and on the top plate with respect to base frame and mobile frame, respectively (12 variables). The joint positions of the three legs in the left half-plane are calculated by symmetry with respect to the y -axis. The unknown variable can be chosen as

$$\mathbf{x} = [a_{x_1} \ a_{y_1} \ a_{x_2} \ a_{y_2} \ a_{x_3} \ a_{y_3} \ b_{x_1} \ b_{y_1} \ b_{x_2} \ b_{y_2} \ b_{x_3} \ b_{y_3}]^T.$$

4.1.4. Griffis-duffy geometry (2+6 variables) – unsymmetric geometry (GD2+6)

The leg attachment points are defined in the Cartesian space and they are constrained on a triangular shape of known side length (see Fig. 6). The variables represent the coordinates a_{x_2} , a_{x_4} , a_{x_6} , b_{x_1} , b_{x_3} , b_{x_5} of the leg attachment points with respect to base plate frame and top plate frame and the sides l_b and l of the

base plate and top plate, respectively. The optimal design, in this case, requires a double optimization process because the bounds of the position coordinate $a_{x_2}, a_{x_4}, a_{x_6}, b_{x_1}, b_{x_3}, b_{x_5}$ variables depend on the computation of the side l_b and l variables. The vector of all the unknown variables can be written as $\mathbf{x} = [l_b \ l \ a_{x_2} \ a_{x_4} \ a_{x_6} \ b_{x_1} \ b_{x_3} \ b_{x_5}]^T$.

$$\begin{aligned}
a_{x_1} &= \frac{l_b}{2}, \quad a_{y_1} = \frac{l_b}{4}\sqrt{3} \\
a_{x_2} &= a_{x_1}, \quad a_{y_2} = \frac{l_b}{4}\sqrt{3} \\
a_{x_3} &= -\frac{l_b}{2}, \quad a_{y_3} = \frac{l_b}{4}\sqrt{3} \\
a_{x_4} &= a_{x_4}, \quad a_{y_4} = -\sqrt{3}\left(\frac{l_b}{4} + a_{x_4}\right) \\
a_{x_5} &= 0, \quad a_{y_5} = -\frac{l_b}{4}\sqrt{3} \\
a_{x_6} &= a_{x_6}, \quad a_{y_6} = \sqrt{3}\left(a_{x_6} - \frac{l_b}{4}\right) \\
b_{x_1} &= b_{x_1}, \quad b_{y_1} = \sqrt{3}\left(b_{x_1} - \frac{l}{4}\right) \\
b_{x_2} &= \frac{l}{2}, \quad b_{y_2} = \frac{l}{4}\sqrt{3} \\
b_{x_3} &= b_{x_3}, \quad b_{y_3} = \frac{l}{4}\sqrt{3} \\
b_{x_4} &= -\frac{l}{2}, \quad b_{y_4} = \frac{l}{4}\sqrt{3} \\
b_{x_5} &= b_{x_5}, \quad b_{y_5} = -\sqrt{3}\left(\frac{l}{4} + b_{x_5}\right) \\
b_{x_6} &= 0, \quad b_{y_6} = -\frac{l}{4}\sqrt{3}.
\end{aligned} \tag{3}$$

base and top plates, respectively; β and γ are the angles that define the deviation of the leg attachment points on the mobile plate from $0\text{--}120\text{--}240^\circ$. The unknown variable vector is $\mathbf{x} = [\beta \ \gamma \ \rho_{b_{ext}} \ \rho_{b_{int}} \ \rho_{ext} \ \rho_{int}]^T$. The leg attachment point positions, with respect to the base plate frame and top plate frame, can be computed in the Cartesian space as a function of the defined parameters as reported below:

$$\begin{aligned}
a_{x_1} &= \rho_{b_{ext}} \cos(0), \quad a_{y_1} = \rho_{b_{ext}} \sin(0) \\
a_{x_2} &= \rho_{b_{ext}} \cos\left(\frac{2\pi}{3}\right), \quad a_{y_2} = \rho_{b_{ext}} \sin\left(\frac{2\pi}{3}\right) \\
a_{x_3} &= \rho_{b_{ext}} \cos\left(\frac{4\pi}{3}\right), \quad a_{y_3} = \rho_{b_{ext}} \sin\left(\frac{4\pi}{3}\right) \\
a_{x_4} &= \rho_{b_{int}} \cos(0), \quad a_{y_4} = \rho_{b_{int}} \sin(0) \\
a_{x_5} &= \rho_{b_{int}} \cos\left(\frac{2\pi}{3}\right), \quad a_{y_5} = \rho_{b_{int}} \sin\left(\frac{2\pi}{3}\right) \\
a_{x_6} &= \rho_{b_{int}} \cos\left(\frac{4\pi}{3}\right), \quad a_{y_6} = \rho_{b_{int}} \sin\left(\frac{4\pi}{3}\right) \\
b_{x_1} &= \rho_{ext} \cos(-\beta), \quad b_{y_1} = \rho_{ext} \sin(-\beta) \\
b_{x_2} &= \rho_{ext} \cos\left(\frac{2\pi}{3} - \beta\right), \quad b_{y_2} = \rho_{ext} \sin\left(\frac{2\pi}{3} - \beta\right) \\
b_{x_3} &= \rho_{ext} \cos\left(\frac{4\pi}{3} - \beta\right), \quad b_{y_3} = \rho_{ext} \sin\left(\frac{4\pi}{3} - \beta\right) \\
b_{x_4} &= \rho_{int} \cos(\gamma), \quad b_{y_4} = \rho_{int} \sin(\gamma) \\
b_{x_5} &= \rho_{int} \cos\left(\frac{2\pi}{3} + \gamma\right), \quad b_{y_5} = \rho_{int} \sin\left(\frac{2\pi}{3} + \gamma\right) \\
b_{x_6} &= \rho_{int} \cos\left(\frac{4\pi}{3} + \gamma\right), \quad b_{y_6} = \rho_{int} \sin\left(\frac{4\pi}{3} + \gamma\right).
\end{aligned} \tag{4}$$

4.1.5. MSP (6 variables) – unsymmetric geometry (MSP6)

The leg attachment points are placed on two circles at both base plate and top plate: three of the six legs are positioned on an inner circle both at the base and mobile platforms, and the other three legs on an outer (concentric) circle (Fig. 7). The leg attachment points on the base plate are fixed and positioned at 120° from each other. So, two variables are used to define the leg attachment points on the base plate and four variables are used to define the leg attachment points on the top plate. In particular, $\rho_{b_{int}}$ and $\rho_{b_{ext}}$, ρ_{int} , ρ_{ext} are the inner and outer circle radii of the

5. The optimization algorithm

An optimization algorithm has been used to combine two different objectives by properly defining a cost function to minimize. In order to minimize the maximum leg force value and to equally distribute among the legs the forces exerted by the linear actuators during a positioning and/or machining task, the maximum RMS value of the forces has been selected as a metric. A second

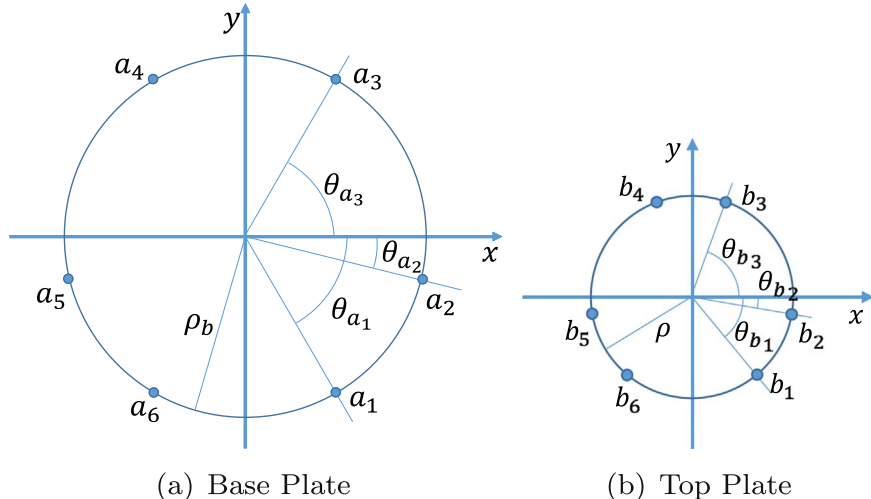


Fig. 4. Stewart-Gough platform 8 variables (unsymmetric) geometry.

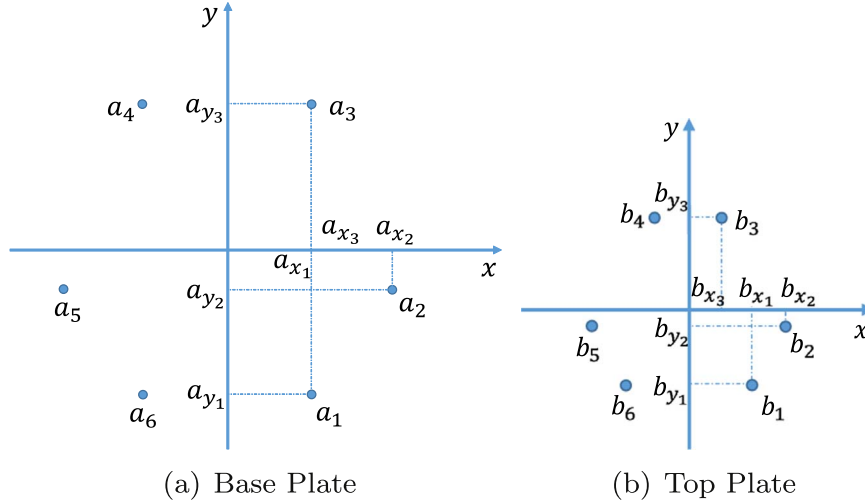


Fig. 5. Generic one axis symmetry (unsymmetric) geometry.

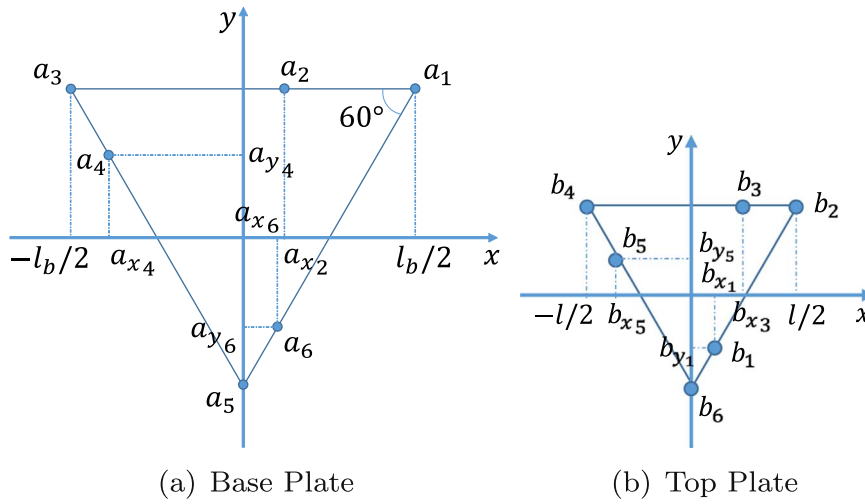


Fig. 6. Griffis-Duffy (unsymmetric) geometry.

objective has been taken into account to maximize (or do not penalize) the robot workspace volume.

5.1. Cost function definition

The cost function $F(\mathbf{x})$ to minimize can be defined as in (5), where the parameters k_1 and k_2 are positive scalar gains which determine the weight of each partial objective in $F(\mathbf{x})$:

$$F(\mathbf{x}) = k_1 W_1(\mathbf{x}) + k_2 W_2(\mathbf{x}). \quad (5)$$

The first contribution $W_1(\mathbf{x})$ takes into account the leg forces necessary to follow a given position and orientation trajectory of the mobile plate that depends on the specific application, e.g. a part positioning during an assembly process, and withstanding of external forces applied to the top plate, e.g. during the handling of a part subject to a machining process. The contribution $W_2(\mathbf{x})$ takes into account the workspace volume. A possible choice of the two terms $W_1(\mathbf{x})$ and $W_2(\mathbf{x})$ can be as in (6), where τ_k is the vector of the leg forces at the k th time instant of the task execution and V_W is the volume of the robot workspace for a given design:

$$W_1(\mathbf{x}) = \frac{1}{N} \sum_{k=1}^N \|\boldsymbol{\tau}_k(\mathbf{x})\|, \quad W_2(\mathbf{x}) = -V_W(\mathbf{x}). \quad (6)$$

The leg forces are computed by solving the inverse dynamics of the Stewart platform, using as input the leg positions, velocities and accelerations computed by solving the IK problem given the desired top plate trajectory. The platform workspace volume is computed by considering the geometrical approach proposed by [65]. In particular, the considered workspace is the positional workspace (or fixed-orientation workspace), computed by maintaining the top plate orientation equal to the base plate orientation. The choice of such $W_1(\mathbf{x})$ allows us to reduce the maximum value of the forces required by the actuators and it also allows us to equalize the mean value of the six forces along the entire considered trajectory. The optimization problem can be formally written as in Eq. (7), where \mathbf{x} is the vector of the unknown variables defined in Section 4.1 for each geometries and $\mathcal{X} = \{\mathbf{x}_{min}, \mathbf{x}_{max}\}$ is the search domain. As already discussed, the search domain, namely the variable bounds, should be defined to avoid collisions between the legs, actuators and fixtures during the execution of the task, to satisfy minimum and maximum dimensions of the plates and, then, to optimize the overall encumbrance of the robot.

$$\begin{aligned} & \min_{\mathbf{x}} F(\mathbf{x}) \\ & \text{s.t. } \mathbf{x} \in \mathcal{X}. \end{aligned} \quad (7)$$

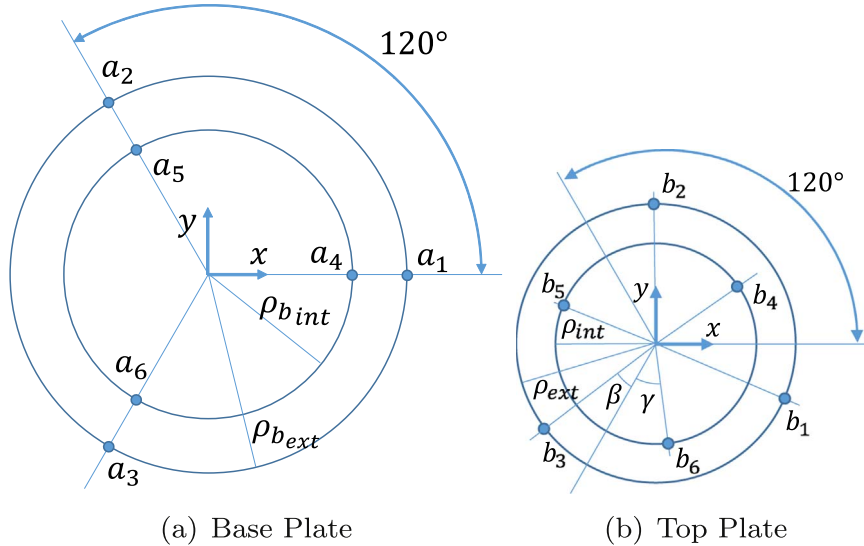


Fig. 7. MSP (unsymmetric) geometry.

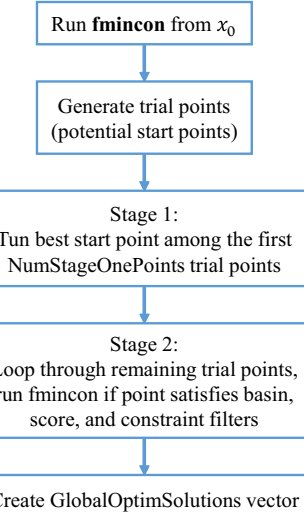
In order to select the most suitable optimization algorithm for the proposed application, the performance of the Genetic, Sequential Quadratic Programming (SQP), stochastic MultiStart and GlobalSearch algorithms were compared. The SQP algorithm is a gradient-based method for solving constrained non-linear optimization problems. The MultiStart is an easy and straightforward algorithm that initiates a local solver from a set of starting points and then creates a vector containing the found local minima, returning the best of these points as the estimated global minimum. The GlobalSearch works similar to the MultiStart but the starting points are generated by a scatter-search mechanism in a more complex way. The algorithm, then, tries to analyse these starting points and discards points that are unlikely to generate a better minimum than the best minimum found so far. The performances of the Multistart algorithm and of the GlobalSearch algorithm have been evaluated by using an Active-Set (AS) algorithm and a SQP algorithm. In other words, from each starting point, an AS algorithm or a SQP algorithm has been executed to find the nearest local minima. Fig. 8 shows a sketch of the GlobalSearch and MultiStart algorithms [66].

Table 1 shows the comparison of the proposed algorithms in the optimization of the SG4 design for the case study I illustrated in Section 6.1. The optimization has been carried out by considering $k_1=0.1$ and $k_2=100$. The algorithms start from the same initial parameter configuration, \mathbf{x}_0 , and they have been evaluated by considering as stopping criteria the minimum function tolerance value set to 10^{-6} . Moreover, the GA algorithm and the SQP algorithm have been tested setting the maximum number of function evaluation (f_{counts}) to 3000, while, the number of the starting points of the MultiStart algorithm has been set to 30. Finally, the GlobalSearch algorithm has been tested by using the parameters NumTrialPoints¹ and NumStageOnePoints² set to 10 000 and 20, respectively. All the proposed setting parameters have been adjusted in successive simulations and they have been chosen so that the algorithms provided the best result. The presented analysis shows that the GA reaches better results than the other algorithms obtaining a smaller value of the cost function F . In fact, although the convergence times

¹ NumTrialPoints is the number of potential start points to examine in addition to \mathbf{x}_0 .

² NumStageOnePoints is the number of points in which the cost function is evaluated. Only in the point with the best score the optimization is carried out. The set of NumStageOnePoints trial points is removed from the list of points to examine.

GlobalSearch Algorithm



MultiStart Algorithm

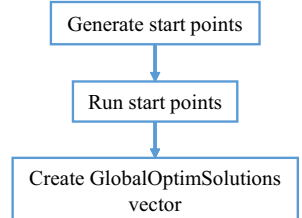


Fig. 8. MultiStart and GlobalSearch algorithm overview.

are not comparable because the SQP algorithm converges in a number of function evaluation counts less than the other ones, it sticks in local minima and, so, it provides a worse design in terms of minimum cost function value. The MultiStart algorithm returns values similar to the GA but a great number of starting points and a larger number of cost function evaluation, and then more time, are required compared to the GA to converge to an optimal value. Finally, the GlobalSearch algorithm does not seem to be suitable for the proposed application given the unsatisfactory results obtained during the optimization process because it sticks in local minima. In conclusion, the GA algorithm appears to be the best choice for the proposed application. Moreover, the use of the AS algorithm, in association with the stochastic algorithm MultiStart, is recommended over the SQP algorithm if a sufficient computational power is not available.

5.2. The genetic algorithm

After a number of simulation trials, the optimization parameters have been set to:

Table 1
Comparison of the optimization algorithms.

Algorithm	F
GA (2280 f_{counts})	-41.2765
SQP (137 f_{counts})	-16.7716
MultiStart AS (3281 f_{counts})	-40.5940
MultiStart SQP (3325 f_{counts})	-38.5824
GlobalSearch AS (147 f_{counts})	-26.2375
GlobalSearch SQP (137 f_{counts})	-16.7716

- Population Size=Number of variables \times 15,
- Number of Generations=50.

The optimization process stops if the maximum number of iterations is reached or if in two successive generations the cumulative change in the fitness function value is less than the termination tolerance value set to be 10^{-6} . The optimization parameters have been chosen so that the optimization algorithm tends to stop for the termination tolerance value criteria ensuring that the GA returns the global minimum (otherwise, it is not guaranteed that the GA finds the best minimum).

For each geometry illustrated in Section 4.1, in order to avoid collisions between the legs, actuators and fixtures, sets of variable boundaries have been properly defined. Moreover, such boundaries have been defined to satisfy other mechanical design constraints, e.g., maximum dimensions of both base and top plates (0.3500 m and 0.1500 m of radius, respectively, in our case), introduced assuming a limited space available for the robot installation. The variable boundaries defined for the considered geometries are reported in Tables 4–8. Moreover, the initial joint positions, the center of gravity (COG) positions of both the base plate and the mobile plate and the COG positions of the work-object fixed to the robot mobile plate, expressed in the world frame, at the instant time $t=0$ are reported in Table 2 and in Table 3, respectively.

Note that the Griffis–Duffy geometry requires a double GA process due to the fact that the leg position variable boundaries have to be computed by using the size of the side of both the base and top plates as described in Section 4.1.4. The optimization time, in this case, necessarily increases. The algorithm scheme is reported in Fig. 9. Only one GA is needed for all the other geometries, instead.

6. Application of the GA based optimization to a realistic scenario

This section describes the results of the optimization process. The optimization of the Stewart platform has been carried out by considering the geometries illustrated in Section 4.1 for the case studies described in Section 6.1. Moreover, in order to compute the workspace volume of the Stewart platform, the motor strokes, and then, the minimum and maximum leg lengths are required. In the proposed simulations a maximum motor stroke of 0.2500 m is considered.

6.1. Case study definition

The optimization process has been carried out by considering two different case studies. The first case study considers a positioning task in which the hexapod moves a work-object along a desired trajectory (for example, simulating a spar positioning or a rib positioning task). The second case study consists of two phases: in the first phase, the hexapod performs a positioning task as in the first case study; in the second phase the hexapod holds the

Table 2
Initial joint positions.

Joint positions	x (m)	y (m)	z (m)
a_1	-0.0850	-0.1472	0.0400
a_2	-0.1700	0	0.0400
a_3	-0.0850	0.1472	0.0400
a_4	0.0850	0.1472	0.0400
a_5	0.1700	0	0.0400
a_6	0.0850	-0.1472	0.0400
b_1	-0.0418	-0.0498	0.4940
b_2	-0.0640	-0.0113	0.4940
b_3	-0.0222	0.0611	0.4940
b_4	0.0222	0.0611	0.4940
b_5	0.0640	-0.0113	0.4940
b_6	0.0418	-0.0498	0.4940

Table 3
COG points at instant time $t=0$ s.

Part	x (m)	y (m)	z (m)
Base plate	0	0	0.0125
Top plate	0	0	0.5187
Work-object	0	0	0.5680

work-object during a manufacturing process, e.g., a drilling process. In detail, in the positioning task the hexapod moves a work-object of 50 kg weight in a desired position along a desired trajectory. The work-object is attached to the mobile plate through a weld joint simulating a tight grasp. The trajectory is planned in the Cartesian space and it is defined by imposing the initial and final poses of the mobile frame (positioned in the COG point of the top plate and oriented to be parallel to the base frame when the top plate is parallel to the base plate). The robot moves from the initial configuration \mathbf{x}_i to the final configuration \mathbf{x}_f reported in (8) (position expressed in meter and orientation in degrees) in a given time $t=5$ s. The motion timing law is of third order polynomial type. By computing the inverse kinematics of the robot, the leg lengths have been computed and the inverse dynamics of the hexapod was solved by controlling the position of each linear actuator:

$$\begin{aligned} \mathbf{x}_i &= [0, 0, 0.5125, 0, 0, 0]^T \mathbf{x}_f \\ &= [0.0064, -0.0043, 0.6930, 8, -3, -1]^T. \end{aligned} \quad (8)$$

In the second case study, when the mobile plate reaches the final pose, the manufacturing task starts. The hexapod holds the work-object fixed in the final position and a force of 500 N is applied along the x direction at $t=6$ s for 2 s on a given point \mathbf{p}_0 on the object.

This point is reported in Eq. (9), where $WorkObj_{COG_f}$ denotes the final position of the work-object. Fig. 10 shows a graphical representation of the considered system. In particular, the lower spar is held in its final position by the hexapod, strictly coupled with the upper cover, during the overall drilling process:

Table 4
SG4 – variable boundaries.

Variable	Min	Max
ρ_b (m)	0.1500	0.3500
ρ (m)	0.0600	0.2200
θ_{hb} (deg)	11	49
θ_h (deg)	17	43

Table 5
SG8 – variable boundaries.

Variable	Min	Max
ρ_b (m)	0.1500	0.3500
ρ (m)	0.0600	0.2200
θ_{a_1} (deg)	$-90^\circ + \theta_{Bound_b}$	$-30^\circ - \theta_{Bound_b}$
θ_{a_2} (deg)	$-30^\circ + \theta_{Bound_b}$	$30^\circ - \theta_{Bound_b}$
θ_{a_3} (deg)	$90^\circ + \theta_{Bound_b}$	$90^\circ - \theta_{Bound_b}$
θ_{b_1} (deg)	$-90^\circ + \theta_{Bound}$	$-30^\circ - \theta_{Bound}$
θ_{b_2} (deg)	$-30^\circ + \theta_{Bound}$	$30^\circ - \theta_{Bound}$
θ_{b_3} (deg)	$90^\circ + \theta_{Bound}$	$90^\circ - \theta_{Bound}$
θ_{Bound_b} (deg)	11	
θ_{Bound} (deg)	18	

Table 6
OA12 – variable boundaries.

Variable	Min	Max
a_{x_1} (m)	0.0050	0.2450
a_{y_1} (m)	-0.3472	-0.1072
a_{x_2} (m)	0.0700	0.3500
a_{y_2} (m)	-0.1000	0.1000
a_{x_3} (m)	0.0050	0.2450
a_{y_3} (m)	0.1072	0.3472
b_{x_1} (m)	0.0018	0.1818
b_{y_1} (m)	-0.2198	-0.0398
b_{x_2} (m)	0.0240	0.2200
b_{y_2} (m)	-0.0363	0.0487
b_{x_3} (m)	0.0022	0.1722
b_{y_3} (m)	0.0511	0.2111

Table 7
GD2+6 – variable boundaries.

Variable	Min	Max
l_b (m)	0.30	0.70
l (m)	0.20	0.44
a_{x_2} (m)	$-\frac{l_b}{2} + p_{Bound_b}$	$\frac{l_b}{2} - p_{Bound_b}$
a_{x_4} (m)	$-\frac{l_b}{2} + p_{Bound_b} \cos(\frac{\pi}{3})$	$-p_{Bound_b} \sin(\frac{\pi}{6})$
a_{x_6} (m)	$p_{Bound_b} \sin(\frac{\pi}{6})$	$\frac{l_b}{2} - p_{Bound_b} \cos(\frac{\pi}{3})$
b_{x_1} (m)	$p_{Bound} \sin(\frac{\pi}{6})$	$\frac{l}{2} - p_{Bound} \cos(\frac{\pi}{3})$
b_{x_3} (m)	$-\frac{l}{2} + p_{Bound}$	$\frac{l}{2} - p_{Bound}$
b_{x_5} (m)	$\frac{l}{2} + p_{Bound} \cos(\frac{\pi}{3})$	$-p_{Bound} \sin(\frac{\pi}{6})$
p_{Bound_b} (m)	0.04	
p_{Bound} (m)	0.03	

Table 8
MSP6 – variable boundaries.

Variable	Min	Max
$\rho_{b_{int}}$ (m)	0.05	0.18
$\rho_{b_{ext}}$ (m)	0.24	0.35
ρ_{int} (m)	0.05	0.12
ρ_{ext} (m)	0.16	0.22
β (deg)	0	60
γ (deg)	0	60

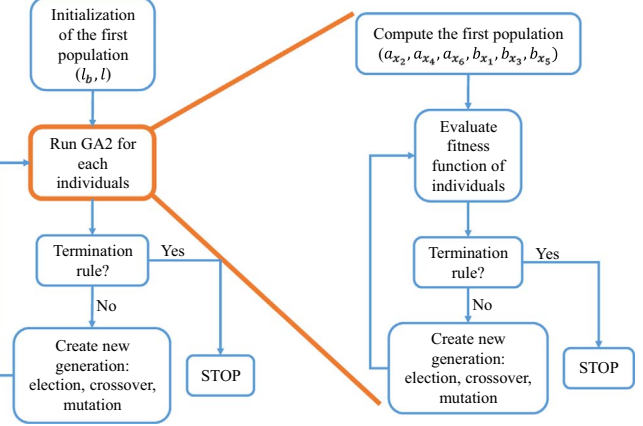


Fig. 9. Genetic algorithms in Griffis-Duffy geometry.

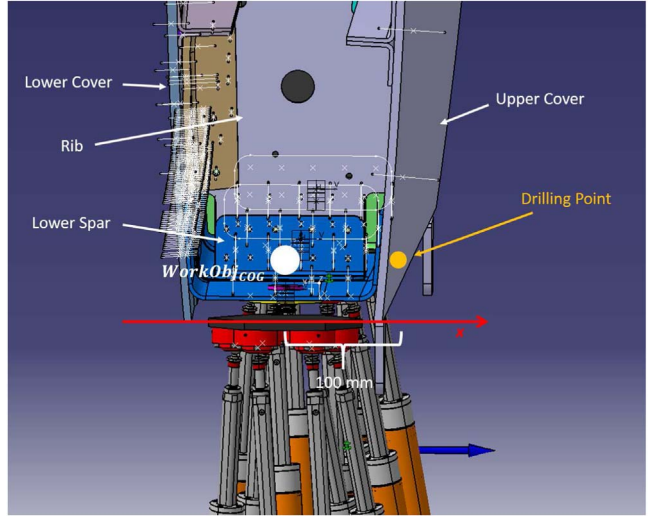


Fig. 10. The considered system during the drilling phase.

$$\mathbf{p}_0 = WorkObj_{COG_f} + [0.1000 \ 0 \ 0]^T. \quad (9)$$

Moreover, the leg force estimation are also compared by defining a second trajectory:

$$\begin{aligned} \mathbf{x}_i &= [0, 0, 0.5125, 0, 0, 0]^T \mathbf{x}_f \\ &= [-0.0053, -0.0137, 0.6938, -8, 5, 3]^T. \end{aligned} \quad (10)$$

In both the trajectories, a z displacement of about 0.181 m is considered. A different orientation is considered, instead. Fig. 11 shows the trajectories of the hexapod top plate.

The results of the optimization process are reported below. The analysis has been carried out by changing the values of the weight parameters k_1 and k_2 in the cost function (5) and by considering a set of initial joint positions obtained from a purely mechanical design accomplished by reducing the overall dimensions of the Stewart platform.

6.2. Obtained results

The simulations were performed by considering two sets of the parameters k_1 and k_2 , i.e., $k_1 = 0.1 - k_2 = 100$ and $k_1 = 0.1 - k_2 = 10$. The first set was considered to optimize the hexapod design with the aim of increasing the robot workspace; the second one, instead, was considered in order to obtain an optimized design which decreases the leg forces exerted by the robot during the assigned task, but still taking

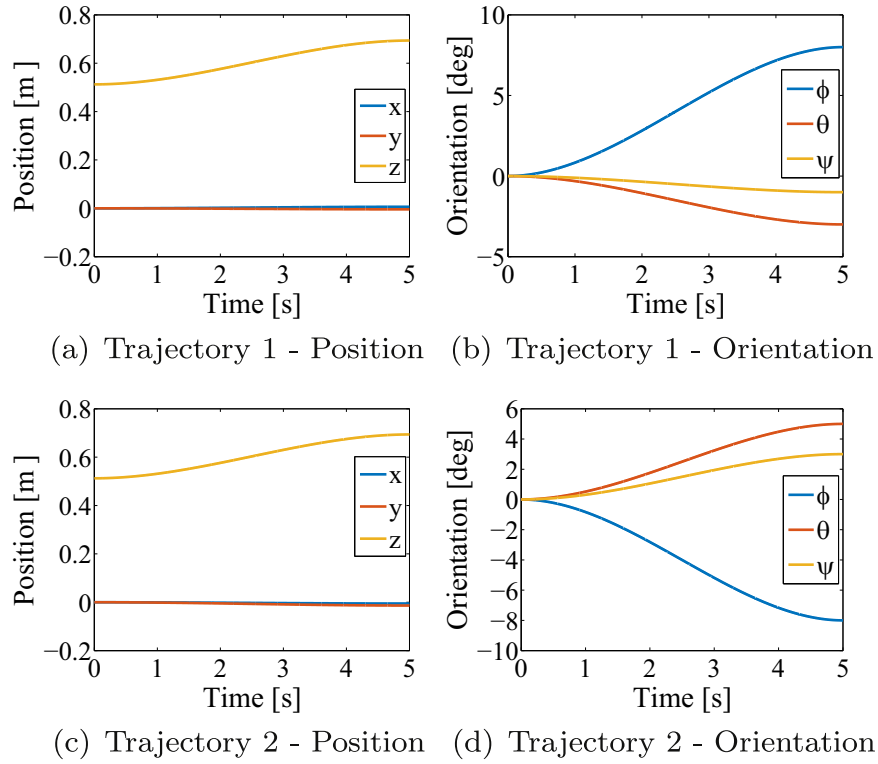


Fig. 11. Top-plate trajectories (position expressed in meter and orientation in degrees).

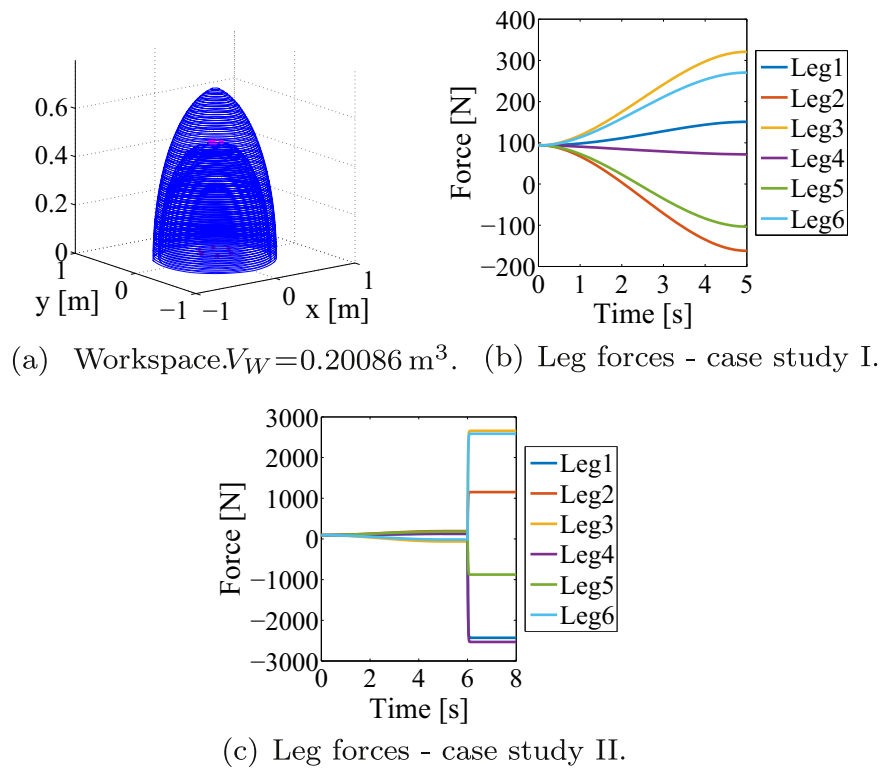


Fig. 12. Initial design.

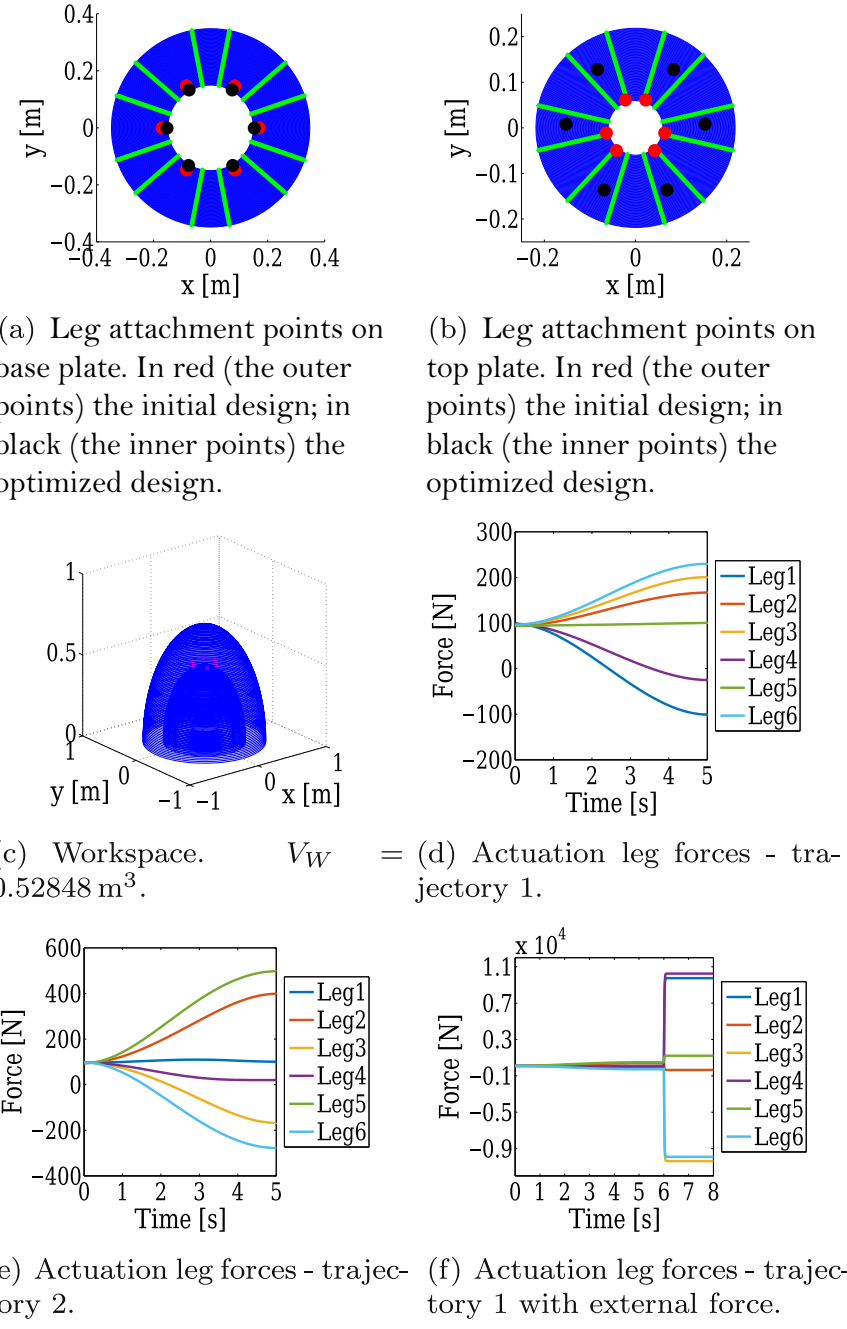


Fig. 13. Stewart-Gough Geometry (4 Variables) – Case study I: $k_1=0.1$, $k_2 = 100$.

into account the workspace volume. In fact, a higher emphasis is given to the leg force contribution W_1 in the cost function F in (5) during the optimization process by decreasing the weight parameter k_2 and, vice versa, a higher emphasis is given to the leg force contribution W_2 in the cost function F by increasing the same parameter k_2 . All the geometries described in Section 4.1 have been analyzed by considering the two sets of parameters. Fig. 12(a) shows the initial workspace of the Stewart platform and Figs. 12(b), (c) show the leg forces required to execute the tasks described above.

The importance of the trajectory in the optimization phase can be understood by analyzing the evolution of the leg forces considering different trajectories as shown in Figs. 13(d), (e) and Figs. 14(d), (e). In the proposed analysis, the SG4

geometry has been optimized along the first trajectory (Section 6.1) by considering the case study I. Let us consider the obtained design. The leg forces estimated along the second trajectory result to be quite different in terms of magnitude and time evolution.

Similarly, the specification of the task strongly affects the optimization process. Let us consider the previous optimized design executing the task specified in the case study II. The estimated leg forces result very high in the manufacturing process although they did not change during the positioning phase as shown in Figs. 13(f) and 14(f). A more suitable design in terms of leg force values can be obtained by considering the manufacturing task in the optimization process. Figs. 15(d) and 16(d) show that an ad hoc

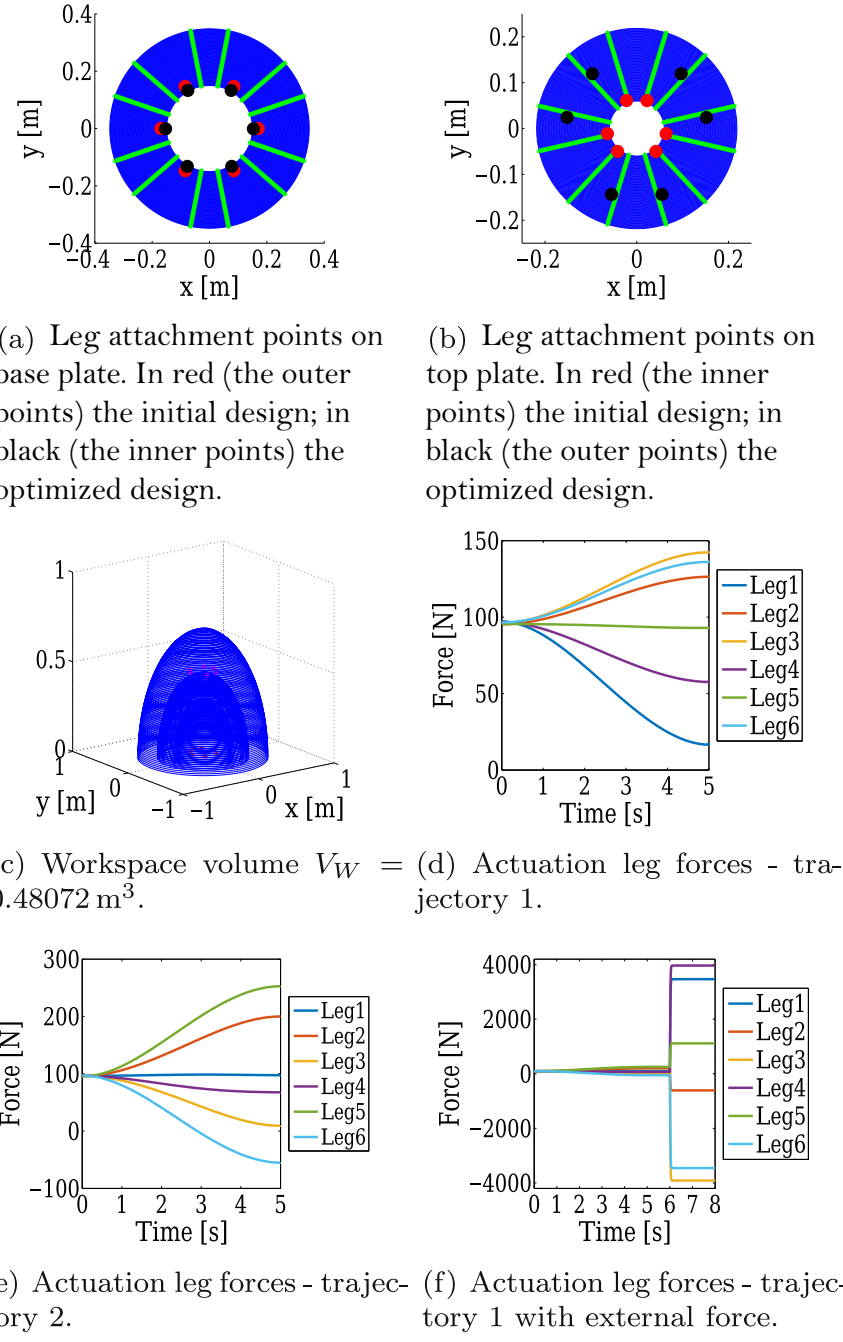


Fig. 14. Stewart-Gough Geometry (4 Variables) – Case study I: $k_1=0.1$, $k_2 = 10$.

design provides better results than the other one reducing the maximum force value of about 55% during the manufacturing task.

The results, furthermore, show that a tailored choice of the mechanical constraints, of the geometry and the parameters used in the optimization process, allows us to obtain an optimal hexapod design that provides a high capability to balance the load of the work-objects and to counteract the external forces during the selected positioning or machining applications while avoiding reduction of the robot workspace volume. Exploiting the anisotropic properties, in fact, a reduction up to 85% of the maximum force required at the actuators compared to the initial proposed design has been obtained.

For brevity, the results obtained by considering all the presented geometries are summarized in Table 9.

6.3. Discussion

By adjusting the weight parameters k_1 and k_2 in (5), the presented tool permits us to obtain an optimized solution tailored to specific applications decreasing significantly the forces exerted by the linear actuators during the task and/or increasing the robot workspace volume. In fact, the reported simulations show that by decreasing the k_2 value, the leg forces and the volume workspace decrease accordingly, or, vice versa, a larger workspace can be obtained by choosing a k_2 larger than k_1 , e.g., SG4-a, although a higher maximum leg force is achieved. Moreover, given the initial design in Fig. 12 that requires a maximum leg force value of about 2650 N and allows us to

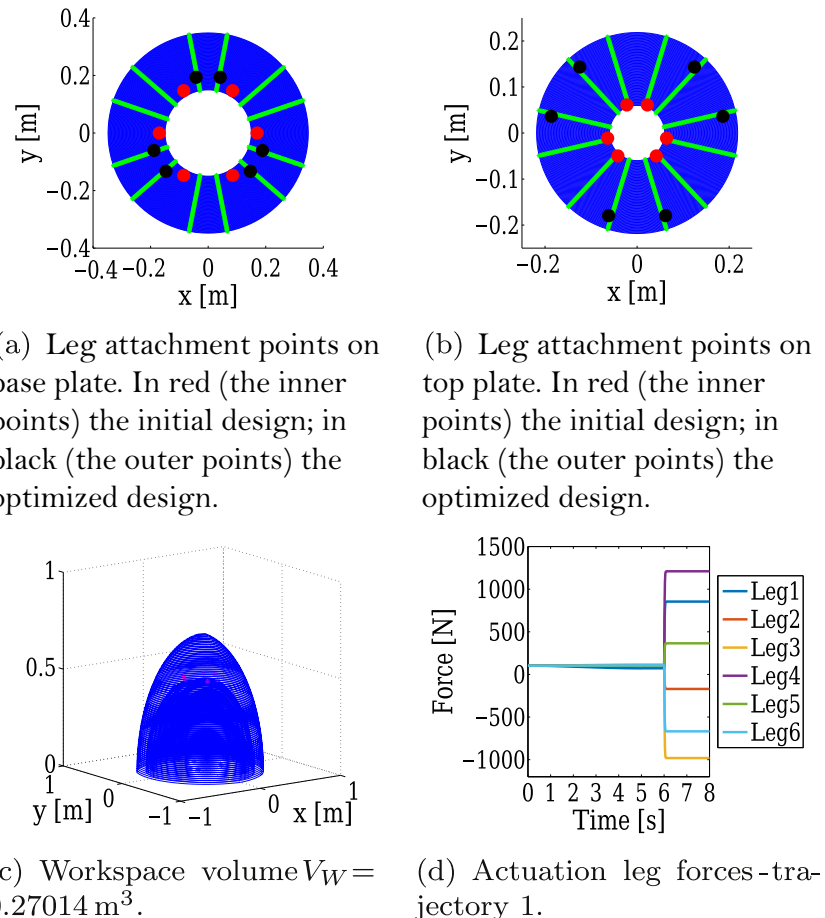


Fig. 15. Stewart-Gough Geometry (4 Variables) – Case study II: $k_1=0.1$, $k_2 = 100$.

obtain a volume of $V_W = 0.20086 \text{ m}^3$, the presented optimized designs surely provide a smaller maximum leg force (up to 85% reduction of the maximum force in the OA12 geometry). This results into a more accurate and cost-effective choice of the mechanical components of the platform. Moreover, the simulations show that the unsymmetric geometries are more useful than the symmetric ones for such applications in which forces tangential to the top plate are considered. In fact, as shown in Table 9, the SG8 and OA12 geometries provide smaller forces than the other ones in the drilling phase (460 N and 489 N, respectively) by keeping the plate dimensions inside the imposed bounds, and, so, by reducing the robot encumbrance inside the flexible fixture.

7. Conclusion

In this work a design approach to support the optimal design of a cost-effective Stewart platform-based mechanisms for manufacturing applications and to facilitate the choice of suitable components for both actuation and mechanical construction was presented. Various symmetric and unsymmetrical geometries have been analysed to show how the optimal design approach can lead to effective results with different robot configurations. Moreover, a comparison between the GA, the SQP algorithm, the MultiStart and the GlobalSearch algorithm has been carried out in order to select the best one in term of minimization accuracy and convergence velocity. The

comparison of the optimization algorithms shows that the GA is the best candidate for the proposed application because the other algorithms stick in local minima, i.e., GlobalSearch and SQP, or require a larger number of starting points and a larger number of cost function evaluation, i.e., MultiStart, than the GA. So, all the proposed simulations have been carried out by using the GA.

The simulation results show that the optimization tool allows us to optimize the hexapod design by decreasing significantly the forces needed to counteract external forces applied to the mobile platform during the selected positioning or manufacturing applications, e.g., drilling, and avoiding reduction of the robot workspace volume. Different from existing work, by exploiting the anisotropic properties of the considered geometries, a reduction up to 85% of the maximum force required at the actuators (compared to the initial design) were obtained while keeping, at the same time, relatively small the size of the platform. The gravity contribution and the forces acting on the robot during the considered tasks, such as drilling forces applied on the work-object attached to the top plate of the hexapod, were considered in the computation of the robot dynamics.

In conclusion, the proposed tool can be used to optimize the design of Stewart platform-based mechanisms and to allow a more accurate and tailored choice of the mechanical components of the robotic platform thus obtaining a real cost-effective solution. Multiple objectives have been pursued: the reduction of the leg forces for the dimensioning of the actuators, the

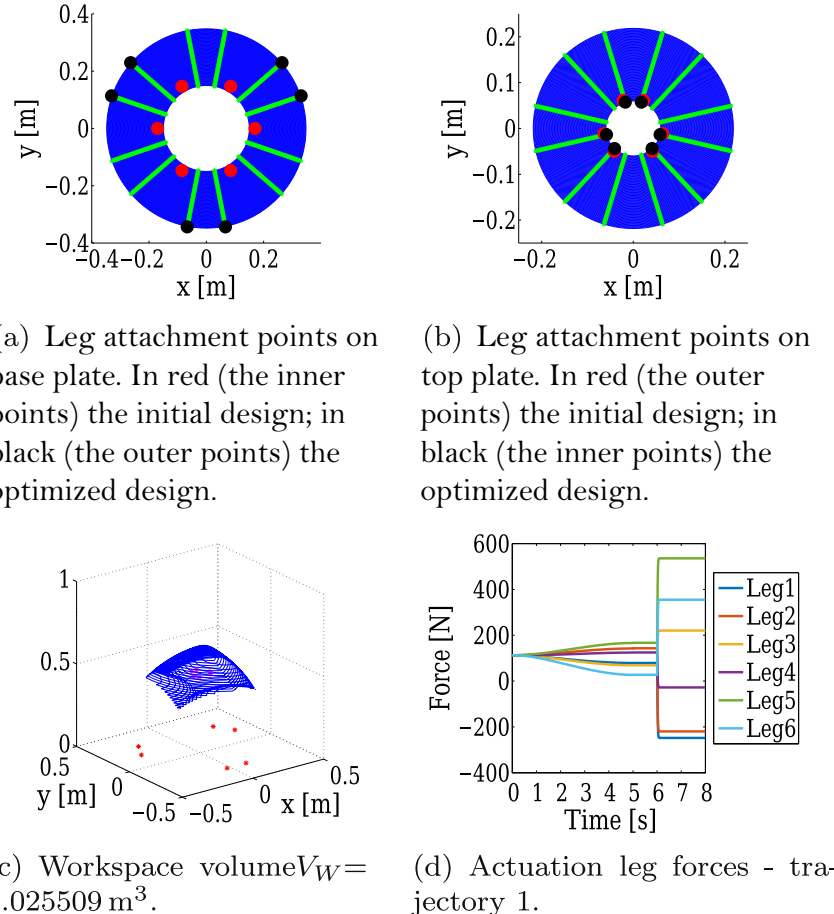


Fig. 16. Stewart–Gough Geometry (4 Variables) – Case study II: $k_1=0.1$, $k_2 = 10$. (For interpretation of the references to color in this figure caption, the reader is referred to the web version of this paper.)

Table 9
Simulation results.

Considered design	Max pos. force (N)	Max man. force (N)	$V_W (\text{m}^3)$
Initial design	194	2650	0.200860
SG4 - Case I: $k_2 = 100$	230	10 400	0.52848
SG4 - Case I: $k_2 = 10$	143	3965	0.48072
SG4 - Case II: $k_2 = 100$	116	1210	0.270140
SG4 - Case II: $k_2 = 10$	167	535	0.025509
SG8 - Case I: $k_2 = 100$	226	–	0.520960
SG8 - Case I: $k_2 = 10$	156	–	0.476040
SG8 - Case II: $k_2 = 100$	149	768	0.193180
SG8 - Case II: $k_2 = 10$	162	460	0.026268
OA12 - Case I: $k_2 = 100$	162	–	0.504220
OA12 - Case I: $k_2 = 10$	141	–	0.459170
OA12 - Case II: $k_2 = 100$	156	1037	0.326830
OA12 - Case II: $k_2 = 10$	144	489	0.032568
GD2+6 - Case I: $k_2 = 100$	435	–	0.231880
GD2+6 - Case I: $k_2 = 10$	343	–	0.0023545
GD2+6 - Case II: $k_2 = 100$	350	748	0.012091
GD2+6 - Case II: $k_2 = 10$	360	658	0.0039947
MSP6 - Case I: $k_2 = 100$	212	–	0.483340
MSP6 - Case I: $k_2 = 10$	157	–	0.435040
MSP6 - Case II: $k_2 = 100$	117	1495	0.250080
MSP6 - Case II: $k_2 = 10$	141	700	0.030380

increasing of the volume of the robot workspace to keep the trajectory inside the robot workspace, and the reduction of the robot dimensions to keep small the encumbrances inside the flexible fixture.

Acknowledgment

This work was supported by the European Commission's Seventh Framework Programme (FP7/2007–2013) under Grant agreement no. 314003 (LOCOMACHS project).

References

- [1] B. Hempstead, R. DeVlieg, R. Mistry, M. Sheridan, Drill and Drive End Effector, SAE Technical Paper 2001-01-2576, 2001.
- [2] R. DeVlieg, K. Sitton, E. Feikert, J. Inman, Once (one-sided cell end effector) Robotic Drilling System, SAE Technical Paper 2002-01-2626, 2002.
- [3] J. Atkinson, J. Hartmann, S. Jones, P. Gleeson, Robotic Drilling System for 737 Aileron, SAE Technical Paper 2007-01-3821, 2007.
- [4] R. DeVlieg, E. Feikert, One-up Assembly with Robots, SAE Technical Paper 2008-01-2297, 2008.
- [5] E. Whinnem, G. Lipczynski, I. Eriksson, Development of orbital drilling for the boeing 787, SAE Int. J. Aerosp. 1(1) (2009) 811–816.
- [6] R. DeVlieg, Robotic Trailing Edge Flap Drilling System, SAE Technical Paper 2009-01-3244, 2009.
- [7] S. Bi, J. Liang, Robotic drilling system for titanium structures, Int. J. Adv. Manuf. Technol. 54 (5–8) (2011) 767–774, <http://dx.doi.org/10.1007/s00170-010-2962-2>.
- [8] P. Ple, J. Gabory, P. Charles, Force controlled robotic system for drilling and riveting one way assembly, SAE Int. J. Aerosp. 4 (2) (2011) 785–788.
- [9] H. Kihlman, M. Engström, Affordable Reconfigurable Tooling, SAE Technical Paper, 2002.
- [10] A. Millar, H. Kihlman, Reconfigurable Flexible Tooling for Aerospace Wing Assembly, SAE Technical Paper 2009-01-3243, 2009.
- [11] D. Simon, L. Kern, J. Wagner, G. Reinhart, A reconfigurable tooling system for producing plastic shields, Procedia CIRP 17 (2014) 853–858.
- [12] P. Kostyrka, J. Kowalsky, Flexible Active and Passive Pogo Fixturing Systems for Aircraft and Aerospace Applications, SAE Technical Paper 2000-01-3012, 2000.
- [13] M. Jonsson, T. Murray, H. Kihlman, Development of an automated

- reconfigurable device for affordable fixturing, in: 21st International Conference on Production Research (ICPR2011), Innovation in Product and Production, 31st July–4th August, Stuttgart, Germany, 2011.
- [14] A.N. Ismail, The design and construction of a 6 degree-of-freedom parallel-link platform type manipulator (Ph.D. thesis), MIT Department of Mechanical Engineering, 1988.
- [15] G.L. Waltman, Black magic and gremlins: analog flight simulations at NASA's flight research center, in: Monographs in Aerospace History, vol. 20, 2000.
- [16] Z. Du, R. Shi, W. Dong, A piezo-actuated high-precision flexible parallel pointing mechanism: conceptual design, development, and experiments, *IEEE Trans. Robot.* 30 (1) (2014) 131–137.
- [17] Y. Su, B. Duan, C. Zheng, Genetic design of kinematically optimal fine tuning stewart platform for large spherical radio telescope, *Mechatronics* 11 (7) (2001) 821–835.
- [18] M. Girone, G. Burdea, M. Bouzit, V. Popescu, J.E. Deutsch, A stewart platform-based system for ankle telerehabilitation, *Auton. Robots* 10 (2) (2001) 203–212.
- [19] K. Hashimoto, Y. Sugahara, H.-o. Lim, A. Takanishi, Optimization design of a stewart platform type leg mechanism for biped walking vehicle, in: M. Kaneko, Y. Nakamura (Eds.), *Robotics Research*, Springer Tracts in Advanced Robotics, vol. 66, Springer, Berlin, Heidelberg, 2011, pp. 169–178.
- [20] J.P. Conti, C.M. Clinton, G. Zhang, A.J. Wavering, Workspace variation of a hexapod machine tool, Citeseer, 1998.
- [21] S.M. Satya, P.M. Ferreira, M.W. Spong, Hybrid control of a planar 3-dof parallel manipulator for machining operations, in: *Transactions-North American Manufacturing Research Institution of SME*, 1995, pp. 273–280.
- [22] A. Marino, P. Cirillo, C. Natale, P. Chiaccio, S. Pirozzi, A general low-cost and flexible architecture for robotized drilling in aircraft assembly lines, in: 2016 International Symposium on Power Electronics, Electrical Drives, Automation and Motion, 2016.
- [23] D.E. Goldberg, *Genetic Algorithms in Search, Optimization and Machine Learning*, 1st Edition, Addison-Wesley Longman Publishing Co., Inc., Boston, MA, USA, 1989.
- [24] J.R. Koza, *Genetic Programming: On the Programming of Computers by Means of Natural Selection*, MIT Press, Cambridge, MA, USA, 1992.
- [25] R. Fletcher, *Practical Methods of Optimization*, 2nd Edition, Wiley-Interscience, New York, NY, USA, 1987.
- [26] P. Gill, W. Murray, M. Wright, *Practical Optimization*, Academic Press, Bingley, Regno Unito, 1981.
- [27] W. Hock, K. Schittkowski, A comparative performance evaluation of 27 nonlinear programming codes, *Computing* 30 (4) (1983) 335–358.
- [28] M. Powell, Variable metric methods for constrained optimization, in: R. Glowinski, J. Lions, I. Laboria (Eds.), *Computing Methods in Applied Sciences and Engineering*, 1977, I, Lecture Notes in Mathematics, Vol. 704, Springer, Berlin, Heidelberg, 1979, pp. 62–72.
- [29] Z. Ugray, L. Lasdon, J. Plummer, F. Glover, J. Kelly, R. Martí, Scatter search and local nlp solvers: a multistart framework for global optimization, *INFORMS J. Comput.* 19 (3) (2007) 328–340.
- [30] F. Glover, A template for scatter search and path relinking, in: *Lecture Notes in Computer Science*, vol. 1363, 1998, pp. 13–54.
- [31] L. Dixon, G.P. Szeg, The global optimization problem: an introduction, in: *Towards Global Optimisation*, vol. 2, 1978.
- [32] R.S. Stoughton, T. Arai, A modified stewart platform manipulator with improved dexterity, *IEEE Trans. Robot. Autom.* 9 (2) (1993) 166–173.
- [33] R. Neugebauer, W.-G. Drossel, C. Harzbecker, S. Ihlenfeldt, S. Hensel, Method for the optimization of kinematic and dynamic properties of parallel kinematic machines, *CIRP Ann.-Manuf. Technol.* 55 (1) (2006) 403–406.
- [34] M. Ceccarelli, G. Carbone, E. Ottaviano, Multi criteria optimum design of manipulators, *Bull. Polish Acad. Sci. Tech. Sci.* 53 (2005).
- [35] F. Hao, J.-P. Merlet, Multi-criteria optimal design of parallel manipulators based on interval analysis, *Mech. Mach. Theory* 40 (2) (2005) 157–171.
- [36] B.J. Lv, S. Zhu, J. Xing, Multi-criteria optimal design of parallel manipulators based on natural frequency, *Appl. Mech. Mater.* 29 (2010) 2435–2442.
- [37] J. Cabrera, F. Nadal, J. Munoz, A. Simon, Multiobjective constrained optimal synthesis of planar mechanisms using a new evolutionary algorithm, *Mech. Mach. Theory* 42 (7) (2007) 791–806.
- [38] A. Rao, P. Rao, S. Saha, Dimensional design of hexaslides for optimal workspace and dexterity, *IEEE Trans. Robot.* 21 (3) (2005) 444–449.
- [39] M. Laribi, L. Romdhane, S. Zeghloul, Analysis and dimensional synthesis of the delta robot for a prescribed workspace, *Mech. Mach. Theory* 42 (7) (2007) 859–870.
- [40] A. Kosinska, M. Galicki, K. Kedzior, Designing and optimization of parameters of delta-4 parallel manipulator for a given workspace, *J. Robot. Syst.* 20 (9) (2003) 539–548.
- [41] K. Miller, Maximization of workspace volume of 3-dof spatial parallel manipulators, *J. Mech. Des.* 124 (2) (2002) 347–350.
- [42] Y. Yang, J.F. O'Brien, A sequential method for the singularity-free workspace design of a three legged parallel robot, *Mech. Mach. Theory* 45 (11) (2010) 1694–1706.
- [43] Y. Yang, J.F. O'Brien, A sequential method for the singularity free workspace design of a planar 3-arm parallel robot, in: *IEEE/RSJ International Conference on Intelligent Robots and Systems*, 2008. IROS 2008, IEEE, Nice, France, 2008, pp. 1977–1982.
- [44] H. Li, C.M. Gosselin, M.J. Richard, Determination of the maximal singularity-free zones in the six-dimensional workspace of the general Gough–Stewart platform, *Mech. Mach. Theory* 42 (4) (2007) 497–511.
- [45] A. Hay, J. Snyman, Methodologies for the optimal design of parallel manipulators, *Int. J. Numer. Methods Eng.* 59 (1) (2004) 131–152.
- [46] S. Bai, Optimum design of spherical parallel manipulators for a prescribed workspace, *Mech. Mach. Theory* 45 (2) (2010) 200–211.
- [47] X.-J. Liu, J. Wang, K.-K. Oh, J. Kim, A new approach to the design of a delta robot with a desired workspace, *J. Intell. Robot. Syst.* 39 (2) (2004) 209–225.
- [48] D. Zhang, Z. Xu, C.M. Mechebske, F. Xi, Optimum design of parallel kinematic toolheads with genetic algorithms, *Robotica* 22 (1) (2004) 77–84.
- [49] D. Zhang, C.M. Gosselin, Kinetostatic analysis and design optimization of the tricept machine tool family, *J. Manuf. Sci. Eng.* 124 (3) (2002) 725–733.
- [50] Z. Gao, D. Zhang, X. Hu, Y. Ge, Design, analysis, and stiffness optimization of a three degree of freedom parallel manipulator, *Robotica* 28 (03) (2010) 349–357.
- [51] X.-J. Liu, Z.-L. Jin, F. Gao, Optimum design of 3-dof spherical parallel manipulators with respect to the conditioning and stiffness indices, *Mech. Mach. Theory* 35 (9) (2000) 1257–1267.
- [52] C. Gosselin, J. Angeles, The optimum kinematic design of a planar three-degree-of-freedom parallel manipulator, *J. Mech. Des.* 110 (1) (1988) 35–41.
- [53] K.E. Zanganeh, J. Angeles, Kinematic isotropy and the optimum design of parallel manipulators, *Int. J. Robot. Res.* 16 (2) (1997) 185–197.
- [54] H. Chen, W. Chen, J. Liu, Optimal design of stewart platform safety mechanism, *Chin. J. Aeronaut.* 20 (4) (2007) 370–377.
- [55] Y. Zhao, Dimensional synthesis of a three translational degrees of freedom parallel robot while considering kinematic anisotropic property, *Robot. Comput.-Integr. Manuf.* 29 (1) (2013) 169–179.
- [56] I. Mansouri, M. Ouali, The power manipulability a new homogeneous performance index of robot manipulators, *Robot. Comput.-Integr. Manuf.* 27 (2) (2011) 434–449, translational Research Where Engineering Meets Medicine.
- [57] A. Lecours, C. Gosselin, Reactionless two-degree-of-freedom planar parallel mechanism with variable payload, *J. Mech. Robot.* 2 (4) (2010) 041010.
- [58] G. Alici, B. Shirinzadeh, Optimum dynamic balancing of planar parallel manipulators based on sensitivity analysis, *Mech. Mach. Theory* 41 (12) (2006) 1520–1532.
- [59] D. Ilia, R. Sinatra, A novel formulation of the dynamic balancing of five-bar linkages with applications to link optimization, *Multibody Syst. Dyn.* 21 (2) (2009) 193–211.
- [60] Y. Zhao, F. Gao, X. Dong, X. Zhao, Dynamics analysis and characteristics of the 8-pss flexible redundant parallel manipulator, *Robot. Comput.-Integr. Manuf.* 27 (5) (2011) 918–928.
- [61] Y. Zhao, Dynamic optimum design of a three translational degrees of freedom parallel robot while considering anisotropic property, *Robot. Comput.-Integr. Manuf.* 29 (4) (2013) 100–112.
- [62] K. Gotlib, D. Kovac, T. Vuherer, S. Brezovnik, M. Brezocnik, A. Zver, Velocity anisotropy of an industrial robot, *Robot. Comput.-Integr. Manuf.* 27 (1) (2011) 205–211.
- [63] Y. Zhao, F. Gao, Dynamic formulation and performance evaluation of the redundant parallel manipulator, *Robot. Comput.-Integr. Manuf.* 25 (4) (2009) 770–781.
- [64] J. Borras, F. Thomas, C. Torras, New geometric approaches to the analysis and design of stewart-gough platforms, *IEEE/ASME Trans. Mechatron.* 19 (2) (2014) 445–455.
- [65] C. Gosselin, Determination of the workspace of 6-dof parallel manipulators, *J. Mech. Des.* 112 (3) (1990) 331–336.
- [66] The MathWorks Inc., <http://it.mathworks.com/help/gads/how-globalsearch-and-multistart-work.html>.